Title:

Cell cycle checkpoint activity in the malaria parasite *Plasmodium falciparum*

Running title: Cell cycle checkpoints in *Plasmodium*

Monique K. Johnson[a], Juliana Naldoni[a,b], William H. Lewis[b], Ross F. Waller[b], Catherine J. Merrick[a#]

[a] Department of Pathology, University of Cambridge, Tennis Court Road, Cambridge, CB2 1QP, UK.

[b] Department of Biochemistry, University of Cambridge, Tennis Court Road, Cambridge, CB2 1QW, UK.

Address correspondence to:

Department of Pathology, Cambridge University, Tennis Court Road, Cambridge, CB2 1QP, UK

Tel: (+44) 1223 333330

Email: cjm48@cam.ac.uk

Abstract

Plasmodium spp. have different modes of cell division from most eukaryotes. Little is known about how these are controlled and cell-cycle checkpoints are particularly poorly characterised. However, parasites can arrest their cell cycle when treated with the frontline antimalarial drug artemisinin, and artemisinin-resistant parasites can modulate their cell-cycle progression, so it is important to understand these aspects of *Plasmodium* biology. Here, we show that *P. falciparum* displays

hallmarks of an intra-S-phase checkpoint when exposed to DNA damage, including acute reduction of DNA replication and phosphorylation of a putative damage-marker histone. Compounds that inhibit human checkpoint kinases can inhibit this arrest of DNA replication, and synergise with DNA damage in parasite killing. This suggests the existence of checkpoint kinase activity in *P. falciparum*, yet these kinases have no clear homologues in *Plasmodium* genomes. Their closest homologues are the phosphatidylinositol lipid kinases. We hypothesise that phosphatidylinositol 3-kinase – which is reportedly up-regulated in artemisinin-resistant parasites – may moonlight in this role, and we characterise this essential kinase for the first time via expansion microscopy. Finally, we show that the cryptic checkpoint-kinase activity may also regulate the ring-stage survival phenotype after artemisinin damage, which resembles a G1/S checkpoint. Hence we suggest that checkpoint kinase inhibitors are candidates for synergy with artemisinin.

Importance

Malaria parasites infect red blood cells, wherein they replicate to produce many new parasites. This is unusual because most cells replicate simply by copying their genome and splitting in half (called binary fission) but malaria parasites make ~20 genome copies, then partition them simultaneously into 20 new cells (called schizogony). Here we studied how schizogony is controlled: in particular, are there 'checkpoints'? Checkpoints pause the cycle for repair if the genome is damaged. We found that DNA damage *did* cause checkpoint hallmarks, yet key proteins that enforce this in other cells are absent in malaria parasites. Furthermore, this checkpoint activity may be involved in the response to an antimalarial drug, when parasites pause their cycle before active replication begins. This implies that inhibiting the checkpoint could exacerbate parasite killing by such drugs. Cancer therapies often work like this – by damaging DNA and also preventing the cancer cells from repairing it.

Keywords

Malaria, *Plasmodium,* cell cycle, checkpoint, PI3K

Introduction

Plasmodium falciparum is the most important cause of human malaria, giving rise to over half a million deaths and hundreds of millions of clinical cases per year (1). Besides being a major human pathogen, it is also a highly unusual protozoan organism, distantly related to humans and other model organisms, with distinctive features of cell and molecular biology. One of these is a non-canonical cell cycle. Instead of dividing by binary fission, as in most model organisms, *Plasmodium* parasites divide primarily by schizogony. After invading a host erythrocyte, they execute multiple, asynchronous rounds of genome replication and nuclear division, generating multiple nuclei within the same cytoplasm. This is followed by a relatively synchronous mass cytokinesis event, partitioning ~20 nuclei and organelles into individual merozoites.

The complex events of schizogony are now being dissected in molecular and cellular detail (2-5) but fundamental questions remain about how the process is regulated. Schizogony is not easily mapped onto the cell cycle phases of G1, S, G2 and M. After invading a host cell, the parasite undergoes a pre-replicative growth phase broadly analogous to G1. The haploid genome is then repeatedly replicated in a continuous S-phase without once-and-only-once regulation, generating many new haploid nuclei. Different nuclei cease to replicate at different times, and divide at different times, so there is no well-defined G2 and no single M-phase (3).

Plasmodium replication is not controlled by conventional cyclin-dependent kinase activity (6), nor is it apparently governed by conventional cell cycle checkpoints, which usually operate at the G1/S transition, within S-phase, and at G2/M. Respectively, these checkpoints delay the start of S-phase, arrest replication if DNA damage or replication stress is detected, and prevent mitosis if a genome is incompletely replicated (7). The *Plasmodium* genus, however, encodes no clear homologues of the checkpoint kinases conserved in most eukaryotes (animals, fungi and plants) e.g.

69 *S. cerevisiae* Mec1 and Rad53 or human ATM/ATR and Chk1/Chk2 (6). (By contrast, some parasites
70 in the apicomplexan phylum, like *Toxoplasma*, do retain homologues of the 'master regulators'
71 Mec1/ATM/ATR, which are phosphoinositide-3-kinase-like kinases (PIKKs), and checkpoints are
72 better characterised in *Toxoplasma* (8-10)).

73 Nevertheless, it seems unlikely that *Plasmodium* is entirely without checkpoints. Eukaryotic
74 cells (not only in metazoans, which must guard against cancer, but also protozoans) generally do
75 pause their cell cycles to ensure effective DNA repair. *Plasmodium* encodes most of the known DNA
76 repair pathways (6, 11) and generates relatively low rates of SNPs, indels and translocations during
77 normal replication (12).

78 There is some evidence for a G1/S-like checkpoint: pre-replicative rings can undergo
79 'temporary growth arrest (TGA)' (13) in response to nutritional (14), temperature (15) or
80 antimalarial-drug (16, 17) stresses. TGA is particularly important under stress caused by the
81 antimalarial drug artemisinin, because it can contribute to treatment failure. However, there is no
82 molecular evidence as-yet that conventional checkpoint effectors are involved. A G1/S checkpoint
83 usually involves the cyclin/CDK complexes that drive S-phase entry, influenced positively by growth
84 factors or negatively by damage responsive kinases like PIKKs. TGA in *Plasmodium*, by contrast, is
85 defined only as a 'non-specific stress-response survival mechanism' (13): induced by multiple
86 stresses, possibly via multiple molecular pathways.

87 An intra-S-phase checkpoint should arrest S-phase specifically after DNA damage or
88 replication stress. In *Plasmodium*, the transcriptional cascade that drives the cell cycle can slow
89 down after DNA damage, with DNA repair proteins and chromatin modifications being upregulated
90 (18), but the signals and transducers for any potential checkpoint are unknown. *Plasmodium*
91 generally lacks validated markers for DNA damage and for direct responses to it. Indeed, the multi-
92 nucleate, asynchronous nature of schizogony raises questions about how an intra-S-phase
93 checkpoint should or could be enforced. Replication itself is apparently regulated per-nucleus,

94 probably via individual accumulations of PCNA, together with non-canonical, chromatin-bound CDK-
95 related kinases like CRK4 (19). Nevertheless, diffusible checkpoint kinases, potentially affecting the
96 whole cell, may not be incompatible with schizogony – at least in response to exogenous DNA
97 damage.

98 Finally, a G2/M checkpoint may be entirely absent because some *P. falciparum* mutants
99 perform grossly aberrant genome segregation but still undergo cytokinesis (20). In fact, even in non-
100 mutants, certain phases of the lifecycle produce a high rate of zoids – this occurs particularly
101 gametogenesis, wherein cytokinesis proceeds even if genome replication fails entirely (21, 22).

102 Here, we set out to investigate checkpoint responses to DNA damage in *Plasmodium,* using
103 newly developed molecular and cellular tools. We show that the hallmarks of an S-phase checkpoint
104 do occur in *P. falciparum*, despite the apparent absence of canonical PIKKs.

105 Results

106 Evidence for DNA-damage-responsive checkpoint activity in *P.* 107 *falciparum*

108 We used two complementary tools to investigate the response to DNA damage during S-phase in *P.*
109 *falciparum*, focussing at the levels of DNA and protein. Firstly, we labelled nascent DNA in
110 replicating parasites with a quantifiable modified nucleotide. This tested whether DNA replication
111 would acutely arrest after damage: a hallmark of the intra-S-phase checkpoint (23, 24). Secondly,
112 we measured phosphorylation of histone H2A, which was recently identified as being analogous to
113 histone H2AX phosphorylation in mammalian cells (25). Canonically, H2AX is phosphorylated at
114 chromatin sites of DNA damage (26, 27). H2AX is absent in *Plasmodium*, but the non-variant histone
115 H2A can nevertheless be phosphorylated (25). Importantly, this indicates an *in trans*, kinase-driven,
116 response that is genuinely 'checkpoint-like'.

117 To induce DNA damage, we used the well-characterised alkylating agent methyl methane
118 sulphonate (MMS), which alkylates DNA bases, particularly guanine and adenine (28). In mammalian
119 cells, it induces an intra-S-phase checkpoint (23). In *P. falciparum* parasites, it leads to DNA
120 breakage, as measured by comet assays (29) and concomitantly delays the cell cycle (18), but its
121 effect as a checkpoint inducer has not been explicitly addressed. In the *P. falciparum* 3D7 strain,
122 MMS had a 48h IC_{50} of ~96µM (Fig S1A). Having established this, we performed highly acute assays
123 over just 1-2h, using 10x or 20x IC_{50}, to minimise non-specific or secondary effects. We confirmed
124 that parasites could substantially recover from this level of MMS exposure within one cell cycle,
125 although their maturation was delayed, as reported previously (18), and there was also a reduction
126 in merozoite numbers in mature schizonts (Fig S2).

127 DNA replication was acutely reduced in the 30 minutes following a 30-minute exposure to
128 MMS at 10x or 20x IC_{50}. Some reduction occurred throughout S-phase (~28-36 hours post invasion,
129 hpi) but it was most pronounced when DNA was damaged in early trophozoites at ~32hpi (Fig 1A).
130 Within a similar timeframe, histone H2A phosphorylation was moderately elevated (Fig 1B). We
131 recently reported that several DNA damaging agents, including MMS, could cause H2A
132 phosphorylation (30), but that the upregulation in trophozoite stages was modest – usually less than
133 2-fold over background levels – making it difficult to measure consistently. This was equally true
134 when MMS was used to induce H2A phosphorylation here (Fig 1B). (Previously published work
135 measured H2A phosphorylation in pre-replicative rings exposed to ionising radiation (25), whereas
136 we measured it in actively replicating trophozoites, wherein the background signal may be higher.)
137 Therefore, we chose the replication-reduction assay as a more robust readout for checkpoint activity
138 in subsequent experiments.
139

140 Absence of clear checkpoint mediators in *P. falciparum*

141 When the intra-S-phase checkpoint is triggered in other eukaryotes, both histone phosphorylation
142 and arrested DNA replication are transduced through PIKKs (24, 26). Since Figure 1 shows that these
143 phenotypes also appear in *P. falciparum,* a transducing kinase should be present. However,
144 orthologues of ATM/ATR are not found in the *P. falciparum* genome (6). To test for the presence or
145 loss of such orthologues more thoroughly, we performed an extensive phylogenetic analysis of PIKK
146 homologues throughout apicomplexans and other major eukaryotic lineages (Fig 2). In this analysis,
147 the lipid kinases PI3K and PI4K formed an outgroup relative to all ATM/ATR-like proteins. In
148 eukaryotes, PI3/4Ks are generally the closest relatives of PIKKs (31) and we did not seek to re-
149 establish this (e.g. by surveying apicomplexan genomes for any other kinases resembling PIKKs), we
150 simply sought to establish patterns of PIKK presence/loss in apicomplexans.

151 ATR homologues were found in most apicomplexans, and some – like *T. gondii* – clearly
152 retained homologues of both ATM and ATR. Other apicomplexans, including *Cryptosporidium*,
153 *Babesia* and *Theileria*, had independently lost the ATM homologue, indicating a propensity for loss
154 of PIKKs in Apicomplexa. *Plasmodium* spp., however, had lost both ATM and ATR, retaining no
155 apparent PIKKs at all. The closest PIKK homologues in any *Plasmodium* genome were the lipid
156 kinases PI3K and PI4K (Fig 2, Fig S3), which were also present throughout apicomplexans (32).
157 (*Theileria*, unusually, was found to have lost its PI3K homologue, possibly due to a lifecycle
158 conducted free in the cytoplasm of leukocytes, which may supply this activity.

159 Notably, the closest *Plasmodium* PIKK homologue, PI3K, is reportedly overexpressed in
160 artemisinin resistant parasites (33), which can alter their cell cycle dynamics. Furthermore, a recent
161 analysis of the steady state locations of mature schizont-stage *P. falciparum* proteins by spatial
162 proteomics assigned PI3K as a nucleus-located protein, whereas PI4K was assigned to cytoplasmic
163 transport vesicles (Fig S4A) (34). This is consistent with PI3K having access to nuclear substrates such
164 as histone H2A for phosphorylation. Accordingly we hypothesised that PI3K might moonlight as a
165 checkpoint kinase in *Plasmodium.*

166 *Pf*PI3K is the only phosphoinositide 3-kinase of the six phosphoinositide kinases in
167 *Plasmodium* (32): it is a well-validated, essential lipid kinase (35), with roles in nutrient uptake and
168 vesicle trafficking (36, 37). However, its moonlighting as a protein kinase would not be
169 unprecedented because other PI3Ks can to act on proteins as well as lipids. For example, humans
170 encode a large family of PI3Ks, and their type-1 PI3Ks can phosphorylate protein substrates like
171 cytokine receptors, as well as auto-phosphorylating themselves (38, 39). The sole *Plasmodium*
172 enzyme is a type-3 PI3K, and thus far these are proven only to phosphorylate lipids (35).
173 We sought orthogonal validation of the spatial proteomics via immunofluorescence after
174 raising peptide antibodies to *Pf*PI3K (Fig 3A, Fig S4B, C). The protein appeared in puncta throughout
175 the cytoplasm, consistent with previous work (37) (Fig 3B). This highly dispersed location could
176 obscure any minor nuclear signal, and we did not detect substantial re-location to nuclei upon DNA
177 damage (Fig 3C). We then used expansion microscopy to better resolve the location of *Pf*PI3K,
178 observing that puncta grew more abundant as cells matured, and were densest in an area free of
179 nuclei that is probably the food vacuole – a known hub for vesicle trafficking (Fig 3D). Some *Pf*PI3K
180 was also detected inside nuclei in all cells imaged (Fig 3E, Fig S5). Of note, we recently showed that
181 the ATM and ATR homologues in *Toxoplasma* are likewise dispersed throughout the cell and do not
182 substantially relocate to the nucleus after DNA damage, but they are nevertheless able to mediate
183 checkpoint phenotypes such as histone phosphorylation (40).

184 We attempted to use the same antibodies to immunoprecipitate native *Pf*PI3K with any
185 potential protein substrates, but only a single *Pf*PI3K peptide was detected across several attempts.
186 It is probably highly unstable *in vitro*, or lacking suitable tryptic digest sites, because it was likewise
187 completely undetected, despite its very large size, in two dedicated proteomic studies of the nuclear
188 versus cytoplasmic proteomes in *P. falciparum* (41, 42); and it was only sparsely detected in spatial
189 proteomics (34). Further validation of an intra-nuclear role for *Pf*PI3K would probably require
190 methods focussed less on the kinase itself and more on its targets – such as BioID for proximity-
191 labelling of protein partners (43).

192 ## The mediator of DNA-damage checkpoint responses in *Plasmodium*

193 ## is sensitive to PIKK inhibitors

194 Assuming that a divergent PIKK-like kinase does exist in *P. falciparum*, we attempted to inhibit it with
195 PIKK inhibitors. We chose two compounds with validated specificity for human ATM and ATR
196 respectively (but not for human PI3Ks), KU-55933 and VE-821 (44, 45). If an ATM-like or ATR-like
197 activity existed in *P. falciparum* – either in *Pf*PI3K or elsewhere – these compounds might specifically
198 inhibit it.

199 We first determined their 48h IC_{50} values on *P. falciparum* (3D7 strain): KU-55933 had an IC_{50}
200 in the micromolar range and VE-821, in the nanomolar range (Fig 4A, Fig S1B). Both inhibitors clearly
201 synergised with MMS in a 48h isobologram analysis, particularly strongly in the case of VE-821,
202 suggesting activity in the same pathway (Fig 4B). Control compounds that kill parasites but are not
203 known to cause DNA damage – the antibiotics blasticidin and geneticin – did not synergise with
204 MMS (Fig S6). Furthermore, when parasites were exposed to high-dose MMS (10x IC_{50}, as in Figure
205 1) simultaneously with KU-55933 or VE-821, the inhibitors ablated the acute reduction in DNA
206 replication caused by MMS, whereas co-exposure to the control antibiotic geneticin did not (Fig 4C).
207 In this short 1h assay, we used the PIKK inhibitors at only their 48h IC_{50} levels, to minimise any
208 negative effects from the inhibitors alone. Indeed, within the timeframe of the assay the inhibitors
209 alone did not significantly affect DNA replication (Fig 4C). Overall, these data strongly supported the
210 existence of a cryptic PIKK activity, responsible for a genuine intra-S-phase checkpoint via *in trans*
211 kinase activity.

212 ## The antimalarial drug dihydroartemisinin induces DNA replication

213 ## arrest in *P. falciparum*

214 MMS is a useful, well-characterised DNA-damaging agent, but it is not an antimalarial drug. We
215 were particularly interested in the potential DNA-damaging activity of antimalarial drugs, because if

216 parasites do make checkpoint responses to such drugs, then their antimalarial activity might be
217 potentiated by inhibiting checkpoint kinases. Artemisinin is such a drug: it has non-specific alkylating
218 activity that may affect both proteins and DNA (46, 47). There are similarities between the
219 parasite's response to dihydroartemisinin (DHA, the active metabolite of artemisinin) and MMS in
220 terms of DNA breakage (46, 48), delay in the parasite's transcriptional cascade, and upregulation of
221 DNA repair genes (18). Indeed, we found that DHA induced H2A phosphorylation, at all stages of the
222 cycle but particularly in pre-replicative ring stages (~3-fold upregulation after 4h exposure to IC_{50}
223 DHA, (Fig 5A)). This confirmed that DHA does indeed cause damage that activates a putative histone
224 kinase, and furthermore that it can cause this damage prior to S-phase.

225 Using the replication-reduction assay, we saw that in replicating parasites, DHA caused an
226 acute reduction in nascent DNA replication, similar to MMS (Fig 5B). However, unlike MMS, this was
227 not ablated by the PIKK inhibitors KU-55933 and VE-821. Consistent with this difference, the
228 inhibitors did not synergise with DHA in isobologram analysis (Fig 5C). This suggested that although
229 both DHA and MMS may damage DNA, they differ in either the type of damage or the cellular
230 response thereto in terms of inducing an intra-S-phase checkpoint.
231

232 Ring-stage survival after artemisinin damage is affected by PIKK
233 inhibitors

234 Cell-cycle checkpoint activity in *P. falciparum* may not be limited to an intra-S-phase checkpoint:
235 most eukaryotic cells also operate a G1/S checkpoint, delaying S-phase entry if cells are damaged,
236 starved or stressed. This may be analogous to the 'TGA' arrest or 'dormancy' that occurs in ring-
237 stage parasites after artemisinin treatment (13). We therefore set out to establish whether ring-
238 stage dormancy induced by DHA actually represents a classical, G1/S checkpoint, responsive to the

239 DNA damage caused in ring stages by DHA (as shown in figure 5A), and mediated by a potential PIKK-
240 like kinase.

241 We conducted the ring-stage survival assay (RSA) on parasites treated with DHA in the
242 presence or absence of PIKK inhibitors. In this assay, pre-replicative early-ring-stage parasites are
243 damaged with a pulse of DHA: most of them die, but some successfully arrest and thence survive.
244 The more parasites are able to do this, the higher the subsequent recovery of viable parasites. We
245 reasoned that if successful arrest is due to PIKK-mediated checkpoint activity, then PIKK inhibitors
246 should reduce ring-stage survival. These experiments were conducted in the 3D7 strain and also in
247 the Cambodian strain MRA-1252, derived from a naturally-arising DHA-resistant strain reverted back
248 to a sensitive phenotype by specific correction of the resistance mutation in the *Kelch13* gene (49):
249 its genetic background is otherwise that of a S.E. Asian DHA-resistant line.

250 Both 3D7 and MRA-1252 are highly sensitive to artemisinin, so we used the 'extended
251 recovery ring-stage survival assay' (eRRSA), which detects recovered parasites very sensitively after
252 72h via quantitative PCR (50). Figure 6A shows that PIKK inhibitors, particularly KU-55933, did
253 exacerbate the killing of ring-stage parasites by DHA. Differences were subtle and parallel assays
254 reading the RSA with the less sensitive flow cytometric assessment of live/dead cells likewise
255 showed marginal differences (Fig S7). However, in triplicate eRRSAs on two independent lines, 3D7
256 and MRA-1252, survival trended consistently downwards when DHA was combined with either
257 inhibitor – so the effect, although not strong, was highly reproducible. As above, we minimised any
258 negative effects of the inhibitors themselves by using them at a low level: only half of the 48h IC_{50}.
259 We confirmed that this exposure alone for 6h did not affect parasite survival after 72h (Fig 6B).

260 These RSAs did not show conclusively that 'TGA' after artemisinin damage represents a true
261 G1/S checkpoint but they did suggest that such a checkpoint, mediated by a cryptic PIKK, may
262 contribute to ring-stage survival. Hence, the cryptic PIKK must be active throughout the cell cycle,
263 not only in actively replicating trophozoites.

264 When the same assay was conducted on DHA-resistant parasites (the parent strain of MRA-
265 1252, called MRA-1240) the result differed. As expected, DHA survival was much better in MRA-
266 1240, and PIKK inhibitors had no negative effect on this survival (Fig 6C). There was even a trend
267 towards better growth and DHA survival when MRA-1240 was exposed to PIKK inhibitors (Fig 6D).
268 Hence, when a Kelch13 mutation was present, conferring DHA resistance, any contribution of
269 checkpoint activity to parasite survival was apparently ablated.

270 Artemisinin-resistant parasites are cross-resistant to MMS and VE-
271 821, but not to KU-55933

272 We hypothesised that artemisinin-resistant parasites like MRA-1240 might not require 'G1/S'
273 checkpoint activity to survive DHA damage because they are more efficient at DNA repair. Several
274 mutations in DNA repair genes have been identified in resistant strains (47), although the pathway(s)
275 leading to improved DNA repair are not fully characterised. We checked whether the DHA-resistant
276 line MRA-1240 was cross-resistant to MMS, and its IC_{50} was indeed significantly higher than that of
277 the matched sensitive line MRA-1252 (and also higher than that of 3D7) (Fig 6E, left panel; Fig S1C).
278 Since the point mutation in Kelch13 is the only difference between the two Cambodian MRA lines, a
279 genetic background of enhanced DNA repair cannot fully account for this.

280 Another explanation could be that MRA-1240 has hyper-active checkpoint activity due to
281 Kelch13-associated over-expression of PI3K (33), and that this stimulates hyperactive DNA repair.
282 This explanation *would* be consistent with the Kelch13 mutant and revertant having different
283 sensitivities to MMS. If so, the Kelch13 mutant state would also be expected to correlate with
284 reduced sensitivity to PIKK inhibitors. Indeed, MRA-1240 was much less sensitive to the VE-821
285 inhibitor (Fig 6E, middle panel; Fig S1C) – so much so that it was difficult to measure a consistent IC_{50}
286 via MSF assay. Curiously, however, the same line was not less sensitive to KU-55933 (Fig 6E, right
287 panel; Fig S1C). This was the first instance in which VE-821 and KU-55933 had shown a clear

288 difference in their effects on *P. falciparum.* It may suggest that in the MRA-1240/1252 genetic
289 background (perhaps unlike 3D7), more than one checkpoint protein is required, and that one of the
290 inhibitors has a broader inhibitory spectrum than the other. For example, *Pf*PI3K may indeed
291 moonlight as a checkpoint kinase, uniquely unregulated after Kelch13 mutation and uniquely
292 inhibited by VE-821, whereas *Pf*PI4K and/or other 'off-target' kinases may also be needed when
293 broader-spectrum damage induces more complex checkpoint responses, and KU-55933 may inhibit
294 this broader kinase spectrum.

295 Validating these speculations would require challenging experiments, such as biochemical
296 assays on recombinant PI3/4K proteins (which are ~250kDa in size), or robust conditional
297 manipulation of the two large, essential genes encoding *PfPI3K* and *PfPI4K* in parallel. We did make
298 several attempts to tag the *PfPI3K* gene for conditional knockdown, but the enzyme's active site is
299 encoded at the extreme 3' end and may become mis-folded after 3' tagging, because all our
300 attempts failed. Similar efforts by other groups to tag or manipulate this gene were likewise
301 unsuccessful or gave no phenotype (51, 52), while a recently-published mutant that irreversibly
302 deletes the 3' end of the *PfPI3K* gene was lethal (53). The very large size of the gene (6.6kb) also
303 precludes its overexpression or dominant-negative overexpression, as well as recombinant protein
304 production for enzyme-activity assays. Overall, these large and essential genes proved near-
305 intractable to molecular genetics. Thus, their putative PIKK-like activity was not conclusively
306 evidenced or disproved, but the dual nuclear/cytoplasmic location of *Pf*PI3K does suggest that it
307 could moonlight on nuclear substrates.

308 Discussion

309 This work provides the first evidence that *Plasmodium* parasites during blood-stage schizogony can
310 enforce an intra-S-phase checkpoint. The checkpoint is evidenced by an acute reduction in the rate
311 of DNA replication and increased phosphorylation of histone H2A in a position analogous to the

312 canonical DNA damage marker H2AX. *P. falciparum* was previously shown to slow its cell-cycle
313 progression after DNA damage (18) but it was not clear if this occurred through cell-cycle checkpoint
314 activity (partly because the *Plasmodium* system lacked validated DNA damage markers, signals or
315 transducers thereof). Markers still remain limited – there are, for example, no cyclin markers for
316 cell-cycle phases, and the H2A phosphorylation that was reported as a DNA damage marker in ring
317 stages (25) is, in our hands, a consistent but low-dynamic-range marker in trophozoite stages,
318 probably because background levels of H2A-P are higher in actively-replicating parasites. However,
319 the ability to measure nascent DNA replication in *Plasmodium* (54) does now allow intra-S-phase
320 checkpoint activity to be measured. Thus, we showed that DNA replication was acutely arrested by
321 two distinct alkylating agents, MMS and the antimalarial drug DHA.

322 The transducer(s) of checkpoint activity in *Plasmodium* remain cryptic. *Plasmodium* spp.
323 lack identifiable orthologues of PIKK kinases, in contrast to many apicomplexans including *T. gondii*
324 (40). Nevertheless, such activity is apparently present, because the reduction in replication caused
325 by MMS was ablated by well-validated inhibitors of human PIKKs. Hence it must be induced *in trans*
326 by a kinase-mediated signalling cascade (also consistent with H2A phosphorylation), rather than
327 occurring simply because alkylated DNA bases physically block the replisome. Interestingly, DHA
328 differed from MMS in this respect: it also induced H2A phosphorylation, and it also affected DNA
329 replication, but PIKK inhibitors did not significantly ameliorate this. Possibly the acute effect of DHA
330 – which is a much larger molecule than MMS – *is* primarily to block replisomes via bulky DNA
331 adducts (a documented effect of alkylating agents in human cells (23)). If such adducts cannot be
332 quickly bypassed whether a checkpoint kinase is active or not, then PIKK inhibitors might not
333 ameliorate the acute reduction in DNA replication.

334 Other, more complex, explanations are also possible for the difference in response to MMS
335 versus DHA. For example, slow DNA replication can, in general, stimulate compensatory activation
336 of extra replication origins (55), but when damage to DNA is sensed, checkpoint kinases act *in trans*

337 to suppress such origin firing (23). If checkpoint kinases are inhibited, then extra origins may fire
338 regardless, hence MMS-damaged cells may keep replicating and encountering more damage, so
339 genome replication ultimately fails to complete. This would explain how MMS and PIKK inhibitors
340 ultimately synergise in cell killing. Perhaps the broader-spectrum damage that DHA causes to
341 proteins as well as DNA (46), and/or the oxidative stress that it generates (48) means that
342 compensatory origin firing does not happen, whether a checkpoint is activated or not. Hence PIKK
343 inhibitors would not synergise with DHA in cell killing. To evidence these rather complex
344 hypotheses, precision measurement of DNA replication dynamics at single-molecule resolution after
345 different types of damage will be needed. This has been achieved in human cells (23), and is now in
346 development for *Plasmodium*.

347 Turning to the possibility of a pre-replicative G1/S checkpoint, the evidence for this being
348 mediated by a PIKK-like kinase is tantalising albeit not conclusive. In the RSA, which measures DHA
349 killing of pre-replicative rings, PIKK inhibitors exacerbated parasite killing. The effect was modest, so
350 if a classical (kinase-enforced) G1/S checkpoint does exist, it is probably not the sole defining factor
351 in survival of artemisinin-induced dormancy. Nevertheless, the trend was consistent in triplicate
352 assays across two genetically-distinct DHA-sensitive strains, 3D7 and MRA-1252. Checkpoint kinase
353 activity could therefore help to protect ring-stage cells, perhaps by detecting DNA damage,
354 stimulating repair, and preventing S-phase entry until repair is complete. By contrast, a DHA-
355 resistant strain showed no effect of PIKK inhibitors. This may be because it can already suppress
356 DHA activation in early rings and thus protect itself from DNA damage; or alternatively, it may still
357 sustain some damage, but be rescued by hyperactive DNA repair (47). Consistent with this latter
358 hypothesis, it was recently shown that when *Pf*PI3K is inducibly knocked out in a DHA-resistant
359 Kelch-13 mutant background, the parasites become less DHA resistant – perhaps because they can
360 no longer resist or repair DHA-related DNA damage when the mediating kinase (*Pf*PI3K) is lost (53).

361 If there is indeed hyperactive DNA repair in the MRA-1240 line, it cannot be conferred per se
362 by a DHA-resistant genetic background because the matched strain MRA-1252 was not cross-
363 resistant to MMS, whereas MRA-1240 was. However, it could be because the Kelch13 mutation,
364 uniquely present in MRA-1240, confers hyper-checkpoint activity, thus stimulating hyperactive DNA
365 repair. In any case, these data raise the intriguing possibility that artemisinin drugs could synergise
366 with checkpoint inhibitors in killing ring-stage parasites; the caveat being that this might only work
367 well in sensitive, not resistant, strains.

368 It is an attractive possibility that *Pf*PI3K is the cryptic checkpoint kinase, particularly if
369 Kelch13 mutant strains do contain more *Pf*PI3K (33). However, we were not yet able to prove or
370 disprove this, owing to the extreme difficulty of manipulating the large, essential *PfPI3K* gene.
371 Broad-spectrum inhibitors such as wortmannin were used in previous work (37), but these are slow-
372 killing and unable to separate lipid-kinase from putative protein-kinase activity. We used PIKK
373 inhibitors instead, hoping to isolate a putative protein kinase activity. The fact that our PIKK
374 inhibitors did not synergise with DHA in MSF assays, whereas specific inhibitors of distinct human
375 PI3Ks (i.e. lipid kinases) *have* been reported to do so (56), may suggest that this succeeded, and that
376 VE-821 and KU-55933 do target a distinct activity in *Plasmodium*. Of course, they may affect
377 irrelevant off-targets, i.e. multiple or unexpected kinases, or even non-kinases. As an example, a
378 repurposed human-kinase inhibitor was recently deployed to target the PK6 kinase in *Plasmodium*,
379 but it actually targeted haem detoxification as well (57). More likely, however, is that these
380 inhibitors genuinely inhibit a *Plasmodium* checkpoint kinase – which may reside in *Pf*PI3K, *Pf*PI4K, or
381 another radically divergent protein. *Plasmodium* contains many kinases whose roles are yet-
382 unknown (58), and the *Plasmodium* cell cycle is driven by markedly divergent kinases such as CRK4
383 (59), so it is entirely possible that *Plasmodium* checkpoints are enforced by novel kinase(s) as well.

384 In conclusion, we present new evidence for measurable cell-cycle checkpoint activity in
385 *Plasmodium*. We also raise the considerable challenge of unambiguously identifying its mediators in
386 this divergent eukaryotic parasite.

387 Methods

388 Full Methods as follows are provided as Supplementary material:

389 - Parasite culture & parasite strains
390 - Database sampling and phylogenetic analysis
391 - BrdU Enzyme-linked immunosorbent assay (ELISA)
392 - Immunofluorescence
393 - Immunofluorescence with expansion microscopy
394 - Malaria SYBR Green-1 Fluorescence (MSF) assay
395 - Isobolograms
396 - Ring-stage Survival Assay (RSA)
397 - RSA analysis: qPCR based & flow cytometry-based
398 - Antibody production
399 - Western blotting

400

401 Acknowledgements

402 We thank Dr Holly Matthews for early work on this project, Dr Ibtissam Jabre for help with H2A-P
403 blots, Prof Kai Wengelnik for sharing a PI3K inducible-knockout line, and Profs Marcus Lee and Paul
404 Roepe for helpful early discussions.

405 This work was funded by the European Research Council (ERC) under the European Union's Horizon
406 2020 research and innovation programme (ERC-2016-COG 725126 to CJM); a PhD studentship from

407 the University of Cambridge Department of Pathology to MKJ; a Biotechnology and Biological
408 Sciences Research Council (BBSRC) grant APP54272 to RFW; and a Gordon and Betty Moore
409 Foundation Investigator Award to RFW (https://doi.org/10.37807/GBMF9194). The funders had no
410 role in study design, data collection, interpretation or the decision to submit the work for
411 publication.

412

413 # References

414 1. WHO. 2023. World Malaria Report 2023.
415 2. Klaus S, Binder P, Kim J, Machado M, Funaya C, Schaaf V, Klaschka D, Kudulyte A, Cyrklaff M,
416 Laketa V, Hofer T, Guizetti J, Becker NB, Frischknecht F, Schwarz US, Ganter M. 2022.
417 Asynchronous nuclear cycles in multinucleated Plasmodium falciparum facilitate rapid
418 proliferation. Sci Adv 8:eabj5362.
419 3. McDonald J, Merrick CJ. 2022. DNA replication dynamics during erythrocytic schizogony in
420 the malaria parasites Plasmodium falciparum and Plasmodium knowlesi. Plos Pathogens 18:
421 e1010595.
422 4. Simon CS, Sturmer VS, Guizetti J. 2021. How Many Is Enough? - Challenges of Multinucleated
423 Cell Division in Malaria Parasites. Front Cell Infect Microbiol 11:658616.
424 5. Liffner B, Cepeda Diaz AK, Blauwkamp J, Anaguano D, Frolich S, Muralidharan V, Wilson DW,
425 Dvorin JD, Absalon S. 2023. Atlas of Plasmodium falciparum intraerythrocytic development
426 using expansion microscopy. Elife 12.
427 6. Matthews H, Duffy CW, Merrick CJ. 2018. Checks and balances? DNA replication and the cell
428 cycle in Plasmodium. Parasit Vectors 11:216.
429 7. Zhou BB, Elledge SJ. 2000. The DNA damage response: putting checkpoints in perspective.
430 Nature 408:433-9.
431 8. Hawkins LM, Naumov AV, Batra M, Wang C, Chaput D, Suvorova ES. 2021. Novel CRK-Cyclin
432 Complex Controls Spindle Assembly Checkpoint in Toxoplasma Endodyogeny. mBio
433 13:e0356121.
434 9. Naumov AV, Wang C, Chaput D, Ting LM, Alvarez CA, Keller T, Ramadan A, White MW, Kim K,
435 Suvorova ES. 2022. Restriction Checkpoint Controls Bradyzoite Development in Toxoplasma
436 gondii. Microbiol Spectr 10:e0070222.
437 10. Alvarez CA, Suvorova ES. 2017. Checkpoints of apicomplexan cell division identified in
438 Toxoplasma gondii. PLoS Pathog 13:e1006483.
439 11. Lee AH, Symington LS, Fidock DA. 2014. DNA repair mechanisms and their biological roles in
440 the malaria parasite Plasmodium falciparum. Microbiol Mol Biol Rev 78:469-86.
441 12. Claessens A, Hamilton WL, Kekre M, Otto TD, Faizullabhoy A, Rayner JC, Kwiatkowski D.
442 2014. Generation of antigenic diversity in Plasmodium falciparum by structured
443 rearrangement of Var genes during mitosis. PLoS Genet 10:e1004812.
444 13. Platon L, Menard D. 2024. Plasmodium falciparum ring-stage plasticity and drug resistance.
445 Trends Parasitol 40:118-130.
446 14. Babbitt SE, Altenhofen L, Cobbold SA, Istvan ES, Fennell C, Doerig C, Llinas M, Goldberg DE.
447 2012. Plasmodium falciparum responds to amino acid starvation by entering into a
448 hibernatory state. Proc Natl Acad Sci U S A 109:E3278-87.

449 15. Yuan L, Hao M, Wu L, Zhao Z, Rosenthal BM, Li X, He Y, Sun L, Feng G, Xiang Z, Cui L, Yang Z.
450 2014. Refrigeration provides a simple means to synchronize in vitro cultures of Plasmodium
451 falciparum. Exp Parasitol 140:18-23.
452 16. Bohorquez EB, Juliano JJ, Kim HS, Meshnick SR. 2013. Mefloquine exposure induces cell cycle
453 delay and reveals stage-specific expression of the pfmdr1 gene. Antimicrob Agents
454 Chemother 57:833-9.
455 17. Witkowski B, Lelievre J, Barragan MJ, Laurent V, Su XZ, Berry A, Benoit-Vical F. 2010.
456 Increased tolerance to artemisinin in Plasmodium falciparum is mediated by a quiescence
457 mechanism. Antimicrob Agents Chemother 54:1872-7.
458 18. Gupta DK, Patra AT, Zhu L, Gupta AP, Bozdech Z. 2016. DNA damage regulation and its role
459 in drug-related phenotypes in the malaria parasites. Sci Rep 6:23603.
460 19. Voss Y, Klaus S, Guizetti J, Ganter M. 2023. Plasmodium schizogony, a chronology of the
461 parasite's cell cycle in the blood stage. PLoS Pathog 19:e1011157.
462 20. Absalon S, Dvorin JD. 2021. Depletion of the mini-chromosome maintenance complex
463 binding protein allows the progression of cytokinesis despite abnormal karyokinesis during
464 the asexual development of Plasmodium falciparum. Cell Microbiol 23:e13284.
465 21. Janse CJ, van der Klooster PF, van der Kaay HJ, van der Ploeg M, Overdulve JP. 1986. DNA
466 synthesis in Plasmodium berghei during asexual and sexual development. Mol Biochem
467 Parasitol 20:173-82.
468 22. Matthews H, McDonald J, Totanes FIG, Merrick CJ. 2022. Dynamics of DNA replication during
469 male gametogenesis in the malaria parasite Plasmodium falciparum. Cellular Microbiology
470 doi:doi.org/10.1101/2021.12.18.473304
471 23. Merrick CJ, Jackson D, Diffley JF. 2004. Visualization of altered replication dynamics after
472 DNA damage in human cells. J Biol Chem 279:20067-75.
473 24. Santocanale C, Diffley JF. 1998. A Mec1- and Rad53-dependent checkpoint controls late-
474 firing origins of DNA replication. Nature 395:615-8.
475 25. Goyal M, Heinberg A, Mitesser V, Kandelis-Shalev S, Singh BK, Dzikowski R. 2021.
476 Phosphorylation of the Canonical Histone H2A Marks Foci of Damaged DNA in Malaria
477 Parasites. mSphere 6.
478 26. Helt CE, Cliby WA, Keng PC, Bambara RA, O'Reilly MA. 2005. Ataxia telangiectasia mutated
479 (ATM) and ATM and Rad3-related protein exhibit selective target specificities in response to
480 different forms of DNA damage. J Biol Chem 280:1186-92.
481 27. Rogakou EP, Pilch DR, Orr AH, Ivanova VS, Bonner WM. 1998. DNA double-stranded breaks
482 induce histone H2AX phosphorylation on serine 139. J Biol Chem 273:5858-68.
483 28. Beranek DT. 1990. Distribution of methyl and ethyl adducts following alkylation with
484 monofunctional alkylating agents. Mutat Res 231:11-30.
485 29. Gopalakrishnan AM, Kumar N. 2013. Opposing roles for two molecular forms of replication
486 protein A in Rad51-Rad54-mediated DNA recombination in Plasmodium falciparum. mBio
487 4:e00252-13.
488 30. Craven HM, Nettesheim G, Cicuta P, Blagborough AM, Merrick CJ. 2023. Effects of the G-
489 quadruplex-binding drugs quarfloxin and CX-5461 on the malaria parasite Plasmodium
490 falciparum. Int J Parasitol Drugs Drug Resist 23:106-119.
491 31. Smith GCM, Jackson SP. 2010. Chapter 77 - The PIKK Family of Protein Kinases. Handbook of
492 Cell Signaling (Second Edition), doi:10.1016/B978-0-12-374145-5.00077-2:575-580.
493 32. Hassett MR, Roepe PD. 2018. PIK-ing New Malaria Chemotherapy. Trends Parasitol 34:925-
494 927.
495 33. Mbengue A, Bhattacharjee S, Pandharkar T, Liu H, Estiu G, Stahelin RV, Rizk SS, Njimoh DL,
496 Ryan Y, Chotivanich K, Nguon C, Ghorbal M, Lopez-Rubio JJ, Pfrender M, Emrich S, Mohandas
497 N, Dondorp AM, Wiest O, Haldar K. 2015. A molecular mechanism of artemisinin resistance
498 in Plasmodium falciparum malaria. Nature 520:683-7.

499 34. Chisholm SA, Flores V, Kemp A, Breckels MA, Koreny L, Dos Santos Pacheco N, Barylyuk K,
500 Kuroshchenkova A, Lilley KS, Rayner JC, Waller RF. 2025. The spatial proteome of the
501 Plasmodium falciparum schizont illuminates the composition and evolutionary trajectories
502 of its organelles. BioRxiv doi:10.1101/2025.11.27.690946
503 35. Hassett MR, Sternberg AR, Riegel BE, Thomas CJ, Roepe PD. 2017. Heterologous Expression,
504 Purification, and Functional Analysis of Plasmodium falciparum Phosphatidylinositol 3'-
505 Kinase. Biochemistry 56:4335-4345.
506 36. Tawk L, Chicanne G, Dubremetz JF, Richard V, Payrastre B, Vial HJ, Roy C, Wengelnik K. 2010.
507 Phosphatidylinositol 3-phosphate, an essential lipid in Plasmodium, localizes to the food
508 vacuole membrane and the apicoplast. Eukaryot Cell 9:1519-30.
509 37. Vaid A, Ranjan R, Smythe WA, Hoppe HC, Sharma P. 2010. PfPI3K, a phosphatidylinositol-3
510 kinase from Plasmodium falciparum, is exported to the host erythrocyte and is involved in
511 hemoglobin trafficking. Blood 115:2500-7.
512 38. Thomas D, Powell JA, Green BD, Barry EF, Ma Y, Woodcock J, Fitter S, Zannettino AC, Pitson
513 SM, Hughes TP, Lopez AF, Shepherd PR, Wei AH, Ekert PG, Guthridge MA. 2013. Protein
514 kinase activity of phosphoinositide 3-kinase regulates cytokine-dependent cell survival. PLoS
515 Biol 11:e1001515.
516 39. Foukas LC, Shepherd PR. 2004. Phosphoinositide 3-kinase: the protein kinase that time
517 forgot. Biochem Soc Trans 32:330-1.
518 40. Johnson MK, Chelaghma S, Koreny L, Waller RF, Merrick CJ. 2024. Characterisation of cell
519 cycle checkpoint kinases in Toxoplasma gondii. BioRxiv
520 doi:doi.org/10.1101/2024.09.10.612042;:doi.org/10.1101/2024.09.10.612042.
521 41. Oehring SC, Woodcroft BJ, Moes S, Wetzel J, Dietz O, Pulfer A, Dekiwadia C, Maeser P, Flueck
522 C, Witmer K, Brancucci NM, Niederwieser I, Jenoe P, Ralph SA, Voss TS. 2012. Organellar
523 proteomics reveals hundreds of novel nuclear proteins in the malaria parasite Plasmodium
524 falciparum. Genome Biol 13:R108.
525 42. Briquet S, Ourimi A, Pionneau C, Bernardes J, Carbone A, Chardonnet S, Vaquero C. 2018.
526 Identification of Plasmodium falciparum nuclear proteins by mass spectrometry and
527 proposed protein annotation. PLoS One 13:e0205596.
528 43. Birnbaum J, Scharf S, Schmidt S, Jonscher E, Hoeijmakers WAM, Flemming S, Toenhake CG,
529 Schmitt M, Sabitzki R, Bergmann B, Frohlke U, Mesen-Ramirez P, Blancke Soares A,
530 Herrmann H, Bartfai R, Spielmann T. 2020. A Kelch13-defined endocytosis pathway mediates
531 artemisinin resistance in malaria parasites. Science 367:51-59.
532 44. Reaper PM, Griffiths MR, Long JM, Charrier JD, Maccormick S, Charlton PA, Golec JM, Pollard
533 JR. 2011. Selective killing of ATM- or p53-deficient cancer cells through inhibition of ATR. Nat
534 Chem Biol 7:428-30.
535 45. Hickson I, Zhao Y, Richardson CJ, Green SJ, Martin NM, Orr AI, Reaper PM, Jackson SP, Curtin
536 NJ, Smith GC. 2004. Identification and characterization of a novel and specific inhibitor of the
537 ataxia-telangiectasia mutated kinase ATM. Cancer Res 64:9152-9.
538 46. Ismail HM, Barton V, Phanchana M, Charoensutthivarakul S, Wong MH, Hemingway J, Biagini
539 GA, O'Neill PM, Ward SA. 2016. Artemisinin activity-based probes identify multiple
540 molecular targets within the asexual stage of the malaria parasites Plasmodium falciparum
541 3D7. Proc Natl Acad Sci U S A 113:2080-5.
542 47. Xiong A, Prakash P, Gao X, Chew M, Tay IJJ, Woodrow CJ, Engelward BP, Han J, Preiser PR.
543 2020. K13-Mediated Reduced Susceptibility to Artemisinin in Plasmodium falciparum Is
544 Overlaid on a Trait of Enhanced DNA Damage Repair. Cell Rep 32:107996.
545 48. Gopalakrishnan AM, Kumar N. 2015. Antimalarial action of artesunate involves DNA damage
546 mediated by reactive oxygen species. Antimicrob Agents Chemother 59:317-25.
547 49. Straimer J, Gnadig NF, Witkowski B, Amaratunga C, Duru V, Ramadani AP, Dacheux M, Khim
548 N, Zhang L, Lam S, Gregory PD, Urnov FD, Mercereau-Puijalon O, Benoit-Vical F, Fairhurst

549 RM, Menard D, Fidock DA. 2015. Drug resistance. K13-propeller mutations confer
550 artemisinin resistance in Plasmodium falciparum clinical isolates. Science 347:428-31.
551 50. Davis SZ, Singh PP, Vendrely KM, Shoue DA, Checkley LA, McDew-White M, Button-Simons
552 KA, Cassady Z, Sievert MAC, Foster GJ, Nosten FH, Anderson TJC, Ferdig MT. 2020. The
553 extended recovery ring-stage survival assay provides a superior association with patient
554 clearance half-life and increases throughput. Malar J 19:54.
555 51. Arendse LB, Murithi JM, Qahash T, Pasaje CFA, Godoy LC, Dey S, Gibhard L, Ghidelli-Disse S,
556 Drewes G, Bantscheff M, Lafuente-Monasterio MJ, Fienberg S, Wambua L, Gachuhi S,
557 Coertzen D, van der Watt M, Reader J, Aswat AS, Erlank E, Venter N, Mittal N, Luth MR,
558 Ottilie S, Winzeler EA, Koekemoer LL, Birkholtz LM, Niles JC, Llinas M, Fidock DA, Chibale K.
559 2022. The anticancer human mTOR inhibitor sapanisertib potently inhibits multiple
560 Plasmodium kinases and life cycle stages. Sci Transl Med 14:eabo7219.
561 52. Mukherjee A, Crochetiere ME, Sergerie A, Amiar S, Thompson LA, Ebrahimzadeh Z, Gagnon
562 D, Lauruol F, Bourgeois A, Galaup T, Roucheray S, Hallee S, Padmanabhan PK, Stahelin RV,
563 Dacks JB, Richard D. 2022. A Phosphoinositide-Binding Protein Acts in the Trafficking
564 Pathway of Hemoglobin in the Malaria Parasite Plasmodium falciparum. mBio 13:e0323921.
565 53. Al Monla R, Penzo M, Vallentin A, Lohia R, Vincent J, Berry L, Gomes AR, Cerdan R,
566 Wengelnik K. 2025. PI3-kinase has multiple functions in asexual blood stages of Plasmodium
567 falciparum. Sci Rep 15:16762.
568 54. Merrick CJ. 2015. Transfection with thymidine kinase permits bromodeoxyuridine labelling
569 of DNA replication in the human malaria parasite Plasmodium falciparum. Malar J 14.
570 55. Courtot L, Hoffmann JS, Bergoglio V. 2018. The Protective Role of Dormant Origins in
571 Response to Replicative Stress. Int J Mol Sci 19.
572 56. Mott BT, Eastman RT, Guha R, Sherlach KS, Siriwardana A, Shinn P, McKnight C, Michael S,
573 Lacerda-Queiroz N, Patel PR, Khine P, Sun H, Kasbekar M, Aghdam N, Fontaine SD, Liu D,
574 Mierzwa T, Mathews-Griner LA, Ferrer M, Renslo AR, Inglese J, Yuan J, Roepe PD, Su XZ,
575 Thomas CJ. 2015. High-throughput matrix screening identifies synergistic and antagonistic
576 antimalarial drug combinations. Sci Rep 5:13891.
577 57. Nardella F, Jiang T, Wang L, Bohmer MJ, Chakraborty S, Okombo J, Calla J, Silva TM, Pazicky
578 S, Che J, Jeon J, Vincent E, Boonyalai N, Coyle R, Buchanan MJ, Schaefer S, Chen D, Khan A,
579 Mayville E, De Souza ML, Treat M, Charlton J, Tumwebaze PK, Tjia S, Montejo L, Cover K,
580 Rosenthal PJ, Cooper RA, Bozdech Z, Lee MCS, Chakrabarti R, Desai SA, Fidock DA, Wang J,
581 Gray NS, Winzeler EA, Chakrabarti D. 2025. Plasmodiumfalciparum protein kinase 6 and
582 hemozoin formation are inhibited by a type II human kinase inhibitor exhibiting antimalarial
583 activity. Cell Chem Biol 32:926-941 e23.
584 58. Ward P, Equinet L, Packer J, Doerig C. 2004. Protein kinases of the human malaria parasite
585 Plasmodium falciparum: the kinome of a divergent eukaryote. BMC Genomics 5:79.
586 59. Ganter M, Goldberg JM, Dvorin JD, Paulo JA, King JG, Tripathi AK, Paul AS, Yang J, Coppens I,
587 Jiang RH, Elsworth B, Baker DA, Dinglasan RR, Gygi SP, Duraisingh MT. 2017. Plasmodium
588 falciparum CRK4 directs continuous rounds of DNA replication during schizogony. Nat
589 Microbiol 2:17017.
590 60. Hoang DT, Chernomor O, von Haeseler A, Minh BQ, Vinh LS. 2018. UFBoot2: Improving the
591 Ultrafast Bootstrap Approximation. Mol Biol Evol 35:518-522.
592 61. Safeukui I, Ware RE, Mohandas N, Haldar K. 2023. Simultaneous adjunctive treatment of
593 malaria and its coevolved genetic disorder sickle cell anemia. Blood Adv 7:5970-5981.
594 62. Yang J, Yan R, Roy A, Xu D, Poisson J, Zhang Y. 2015. The I-TASSER Suite: protein structure
595 and function prediction. Nat Methods 12:7-8.

596

597 # Figure legends

598 **Fig 1:** Evidence for DNA-damage-responsive checkpoint activity in *P. falciparum*

599 A. BrdU incorporation into populations of trophozoites at three stages, after treatment with
600 MMS, as measured by ELISA. Parasites were treated with MMS for 1 h and BrdU was added
601 for the latter 30 mins. Means of two biological replicates, conducted in technical triplicate,
602 are shown; error bars show range. MMS treatments: 10x IC_{50}, 960 µM; 20x IC_{50}, 1.92 mM.
603 For each parasite stage, statistical testing was via ordinary one-way ANOVA and posthoc
604 Tukey's multiple comparisons test. *, P-value <0.05; comparisons not shown, ns. Pictures
605 show examples of trophozoites at each timepoint. Scale bar, 2µm.
606 B. Representative western blot of phosphorylated histone in trophozoite parasite lysate
607 treated with MMS (2 h, 10x IC_{50}). Phosphorylated histone signal was quantified versus
608 control histone H4: relative quantification is shown below the blot. Graph shows
609 quantifications from three biological replicate blots, relative to either H4 or Hsp70 as a
610 control protein. Unpaired two-tailed t-test: P-value = 0.0354.
611

612 **Fig 2:** *Plasmodium* encodes no homologues of PIKK checkpoint kinases

613 C. A phylogeny inferred for amino acid protein sequences of ATR, ATM, and TOR homologues
614 sampled from broad eukaryote groups. Apicomplexa homologues of PI3K and PI4K (the most
615 closely related proteins to ATR and ATM present in *Plasmodium*) and characterised
616 homologues of PI3K and PI4K from *Saccharomyces cerevisiae* and *Homo sapiens* were
617 included as an outgroup. Support values, displayed as percentages, were generated from
618 1000 ultrafast bootstrap replicates (60) and only support values ≥ 90, indicating strongly
619 supported clades, are shown. The scale bar represents the number of amino acid
620 substitutions per site. A fully-expanded version of this tree with no collapsed clades and
621 displaying sequence accessions is provided in the source data.
622

623 **Fig 3:** *Pf*PI3K is dispersed throughout the cell and does not visibly relocate to the nucleus upon DNA
624 damage

625 A. Western blots showing detection of *Pf*PI3K by two antisera raised to *Pf*PI3K peptides.
626 Replicate lanes from the same blot of protein lysate from late-stage *P. falciparum* were
627 exposed to either pre-immune or immune serum. Histone H4 was used as a loading control.
628 B. Immunofluorescence assay (IFA) showing location of *Pf*PI3K (detected by antiserum 1) in *P.*
629 *falciparum*. 2 representative cells are shown per stage. Scale bar 1 μm.
630 C. IFA showing *Pf*PI3K in *P. falciparum* after DNA damage: 1 h treatment with 5x or 10x IC_{50} of
631 DHA or MMS on late-stage parasites. One representative cell per condition is shown. Scale
632 bar 1μm.
633 D. IFA showing *Pf*PI3K after expansion: maximum projections of 2-3 representative cells per
634 condition, as in (C). DAPI, blue; *Pf*PI3K, green; scale bar 10μm.
635 E. Single sections from the IFA in (D): nuclear *Pf*PI3K signals are highlighted with arrows. Full Z
636 stacks are shown in supplementary data.
637

638 **Fig 4:** Inhibitors of human PIKKs synergise with the DNA-damaging agent MMS in *P. falciparum*

639 A. Inhibition of parasite growth by VE-821 and KU-55933 (molecular structures of each
640 inhibitor are shown). Growth curves from five independent malaria SYBR green I-based
641 fluorescence (MSF) assays: percentage parasite growth is plotted as a function of drug
642 concentration, error bars are standard errors of the means. Mean IC_{50}s from all experiments
643 are shown (individual IC_{50} values from replicate experiments are in Fig S1B).
644 B. Isobolograms plotted as fractional inhibitory concentrations (FIC) of combinations of MMS
645 and VE-821 or KU-55933, as determined by MSF assay. FIC calculations were completed for
646 each combination by dividing the measured "apparent" IC_{50} values for individual drugs in the
647 different combinations by IC_{50} values obtained when the drugs were used alone. Each curve

648 represents a different biological replicate experiment. The mean FIC ($\Sigma FIC(FIC_A+FIC_B)$) is
649 shown, with range. The type of relationship was defined as moderately synergistic based on
650 well-established criteria: ∑FIC <0.5, substantial synergism; ∑FIC <1, moderate synergism;
651 ∑FIC ≥1 and <2, additive interaction; ∑FIC ≥2 and <4, slight antagonism and ∑FIC >4, marked
652 antagonism (61).

653 C. BrdU incorporation into 30-32 hpi trophozoites after treatment with MMS, VE-821, KU-
654 55933, geneticin and combinations of these, measured by ELISA. Parasites were treated with
655 10x IC_{50} of drug for 1 h and BrdU was added for the latter 30 mins. Six biological replicates
656 are plotted, each completed in technical triplicate. Mean and standard deviation error bars
657 are plotted, values normalised to control (set to 100%) in each replicate. Concentrations of
658 drugs used: MMS 960 μM, VE-821 1.62 μM, KU-55933 400 μM, geneticin 1500 μg/ml.
659 Ordinary one-way ANOVA and posthoc Tukey's multiple comparisons test of control vs all
660 and MMS vs all was completed; P-values: *, <0.05; **, <0.01; ***, <0.001; ****, <0.0001;
661 comparisons not shown, ns.

662

663 **Fig 5:** <u>The antimalarial drug dihydroartemisinin induces a DNA replication arrest in *P. falciparum*</u>

664 A. Western blot of phosphorylated histones in ring, trophozoite and schizont-stage parasites
665 treated with DHA (4h, IC_{50} (3nM)). Phosphorylated histone signal was quantified versus
666 control histone H4: relative quantification is shown below the blot.

667 B. BrdU incorporation into 30-32 hpi trophozoites after treatment with DHA, VE-821, KU-55933
668 and combination treatments. Parasites were treated with 10X IC_{50} of drug for 1 h and BrdU
669 was added for the latter 30 mins. Five biological replicates were plotted, each completed in
670 technical triplicate. Mean and standard deviation error bars are plotted; values were
671 normalised to control (set to 100%) in each replicate. Concentrations of drugs used: DHA 45
672 nM, VE-821 1.62 μM, KU-55933 400 μM. Statistical testing by ordinary one-way ANOVA and

673 posthoc Tukey's multiple comparisons test of control vs all and DHA vs all; P-values: *, <0.05;
674 comparisons not shown, ns.
675 C. Isobolograms plotted as Figure 4B. Each curve is a biological replicate and the mean FIC
676 ($\Sigma FIC(FIC_A+FIC_B)$) is shown, with range. The relationship between DHA and either VE-821 or
677 KU55933was defined as additive.

678

679 **Fig 6**: Ring-stage survival is affected by PIKK inhibitors

680 Data in A-D are from eRRSA assays on the strains 3D7, MRA-1252 and MRA-1240. Samples were
681 treated with DMSO (the control condition), VE-821, KU-55933, DHA and combinations of these. Drug
682 concentrations: VE-821, 81 nM (0.5X IC_{50}); KU-55933, 20 μM (0.5X IC_{50}); DMSO, 0.02%; DHA, 700 nM.
683 Values plotted are the means of -log(foldchange = 2^(DHA-DMSO)) for each treatment. Midline
684 represents the mean and boxes show min to max from three biological replicates, each conducted in
685 technical triplicate. Statistical testing by ordinary one-way ANOVA and Dunnett's multiple
686 comparisons test, comparing all means to the mean value from DMSO- or DHA-treated samples. P-
687 values: *, <0.05; **, <0.01; ***, <0.001; ****, <0.0001. Differences between DHA-treated samples
688 +/- PIKK inhibitors did not reach statistical significance, but the p-values for DHA + VE-821 or DHA +
689 KU-55933 versus control were < 0.0001, rather than 0.001 for DHA-alone versus control.
690 A. Ring-stage DHA-sensitive parasite strains, 3D7 or MRA-1252, were treated with DMSO (control
691 condition), DHA and inhibitors VE-821 or KU-55933 in combination with DHA for a 6 h pulse, then
692 left to recover for 72 h.
693 B. Control experiments without DHA: ring-stage 3D7 or MRA-1252 parasites were treated with
694 DMSO or inhibitors VE-821 or KU-55933 for a 6 h pulse, then left to recover for 72 h.
695 C. Ring-stages of the DHA-resistant parasite strain MRA-1240 were treated with DMSO (control
696 condition), DHA and inhibitors VE-821 or KU-55933 in combination with DHA for a 6 h pulse, then
697 left to recover for 72 h.

698 D. Control experiment without DHA: ring-stage MRA-1240 parasites were treated with DMSO or
699 inhibitors VE-821 or KU-55933 for a 6 h pulse, then left to recover for 72 h.
700 E. Inhibition of growth over a full 48h growth cycle by MMS, VE-821 and KU55933 was measured in
701 the strains 3D7, MRA-1252 and MRA-1240 via MSF assay. IC_{50}s were calculated from at least
702 three independent experiments and all values are plotted, with the midline showing the mean
703 and error bars showing standard deviation. MSF growth curves are in Fig S1C.
704

705 # Supporting information

706 **Fig S1: Growth curves determining IC_{50} values for MMS, VE-821 and KU-55933 in the parasite**
707 **strains 3D7, MRA-1252 and MRC-1240.**

708 Each panel shows growth curves from 3-5 independent malaria SYBR green I-based fluorescence
709 (MSF) assays: percentage parasite growth is plotted as a function of drug concentration; error bars
710 are standard errors of the means.
711 A. Inhibition of growth of 3D7 strain by MMS.
712 B. IC_{50} values from the growth curves shown in main figure 3A.
713 C. Inhibition of strains MRA-1252 and MRA-1240 by the drugs VE-821, KU55933 and MMS.
714

715 **Fig S2: 3D7 parasites survive a short pulse of MMS or DHA at the trophozoite stage, but their**
716 **maturation is delayed and progeny number per schizont, reduced.**

717 A. Images were taken 12h after trophozoites at 30-32hpi had been exposed to a 1 h pulse of
718 10X IC_{50} MMS or DHA (2 independent experiments, '1' and '2'). Images show that at this
719 timepoint (i.e. 42-44hpi), cultures were dominated by a mixture of immature and mature
720 schizonts, without clear evidence of parasite death in the damaged cultures. Parasites were

721 then treated with 75nM ML10 for 10 h, to arrest mature schizonts before egress, and re-
722 imaged. Mature schizonts then dominated in all cultures.
723 B. Parasite stages imaged in (A) were categorised as either: early rings, small rings, large rings,
724 early trophozoites, mid trophozoites, late trophozoites, immature schizonts or mature
725 schizonts (2 independent experiments, n ≥ 100 from each experiment). Differences between
726 the proportions of stages in control vs DHA-treated vs MMS-treated cultures were tested via
727 two-way ANOVA and posthoc Tukey's multiple comparisons test. P-values are shown in a
728 table below the graph: *, <0.05; **, <0.01; ***, <0.001. Stars of matched colours across
729 rows denote a significant difference between those conditions (e.g. at 44hpi, there were still
730 more immature schizonts after MMS treatment than in the control (pink stars); 10h later,
731 this difference disappeared, with more mature and fewer immature schizonts (denoted by
732 pairs of yellow and blue stars). The only other difference was in the small numbers of rings
733 that escaped and reinvaded after prolonged arrest.
734 C. Merozoites per schizont were counted in each of the cultures shown in (A) (n = 26-30 per
735 culture). Numbers of merozoites substantially increased in all cultures after the long ML10-
736 arrest period, which allowed mature schizonts to accumulate even after the damage-
737 induced delay seen in (B). A reduction in merozoite number was, however, still seen after
738 MMS damage, although this was not significant after DHA damage.

739

740 **Fig S3: Protein sequence alignment of *P. falciparum* PI3K, PI4K and PIKKs from *S. cerevisiae* and**
741 **human.**

742 MUSCLE (3.8) alignment of catalytic domains of *P. falciparum* PI3K and PI4K against human ATM,
743 ATR, PI3K, and yeast Mec1 and Tel1. Colour key is ClustalW standard. Highlighted in the yellow boxes
744 are the catalytic loops in ATR and ATM. Percentage identity matrix is shown below the alignment.

745

746 **Fig S4: Predicted cellular locations of *Pf*PI3K and *Pf*PI4K, and anti-PfPI3K antibody production**

747 **A.** Data plotted from (34), highlighting the clusters of *P. falciparum* proteins classified via
748 spatial proteomics as nuclear (yellow) and vesicular (brown). *Pf*PI3K (encoded by gene
749 PF3D7_0515300, red arrow)) is classified as nuclear, but falls at the boundary of the two
750 clusters, whereas *Pf*PI4K (encoded by gene PF3D7_0509800, green arrow) is classified as
751 vesicular and falls in the centre of the vesicular cluster.

752 B. Model made in i-TASSER (62), threading 1500 C-terminal residues of the 2133-amino acid
753 *Pf*PI3K against human ATR. Protein coloured blue to red, N-terminal to C-terminal. Peptides
754 used as antigens are highlighted in white and circled: amino acids 1359-1374 and 2011-2025
755 of full length *Pf*PI3K.

756 C. Controls for specificity of immune versus pre-immune antisera against *Pf*PI3K.
757 Representative images of single cells are shown. Scale bar 1 µm. Primary antibodies used
758 were rabbit antisera, pre-immune or immune, diluted 1:200 in 3% BSA.

759

760 **Fig S5: Immunofluorescence after expansion, showing the location of PfPI3K**

761 Examples of full Z-stacks taken during imaging of expanded cells: these stacks generated the
762 maximum projections shown in Figure 3D for control cell (iii), DHA-treated cell (i) and MMS-treated
763 cell (ii). They include the single sections extracted for Figure 3E. DAPI, blue; *Pf*PI3K, green; scale bar
764 10µm.

765

766 **Fig S6: Isobolograms showing that two antibiotic drugs do not synergise with MMS**

767 Isobolograms plotted as fractional inhibitory concentrations (FIC) of combinations of MMS and
768 geneticin (G-418), or blasticidin (BSD), as determined by MSF assay. Data were processed as in Figure
769 4B. The type of relationship was defined as additive for blasticidin and borderline antagonistic for
770 geneticin, based on well-established criteria (∑FIC <0.5, substantial synergism; ∑FIC <1, moderate

771 synergism; ∑FIC ≥1 and <2, additive interaction; ∑FIC ≥2 and <4, slight antagonism and ∑FIC >4,

772 marked antagonism).

773

774 **Fig S7: Ring stage survival assessed by flow cytometry**

775 A ring-stage survival assay was assessed by flow cytometry as well as eRRSA as used in Figure 5.

776 Density plot quadrant graphs show one biological replicate of an RSA conducted on 3D7. Cell counts

777 for each quadrant are shown. Percentage survival was calculated as the proportion of live versus

778 dead cells (SYBR+ MITO+/SYBR+ MITO-) for each condition.

779

780 **Fig S8: Raw growth-curve data for all isobolograms plotted in figures 4B, 5C and S5**

781 A. Data for isobolgrams in figure 4B, VE-821 with MMS

782 B. Data for isobolgrams in figure 4B, KU-55933 with MMS

783 C. Data for isobolgrams in figure 5C, VE-821 and KU55933 with DHA

784 D. Data for isobolgrams in figure S5, Blasticidin and G-418 with MMS

785

786 **Source data files 1-6**

787 Files 1-6: Source data for phylogenetic tree shown in figure 2

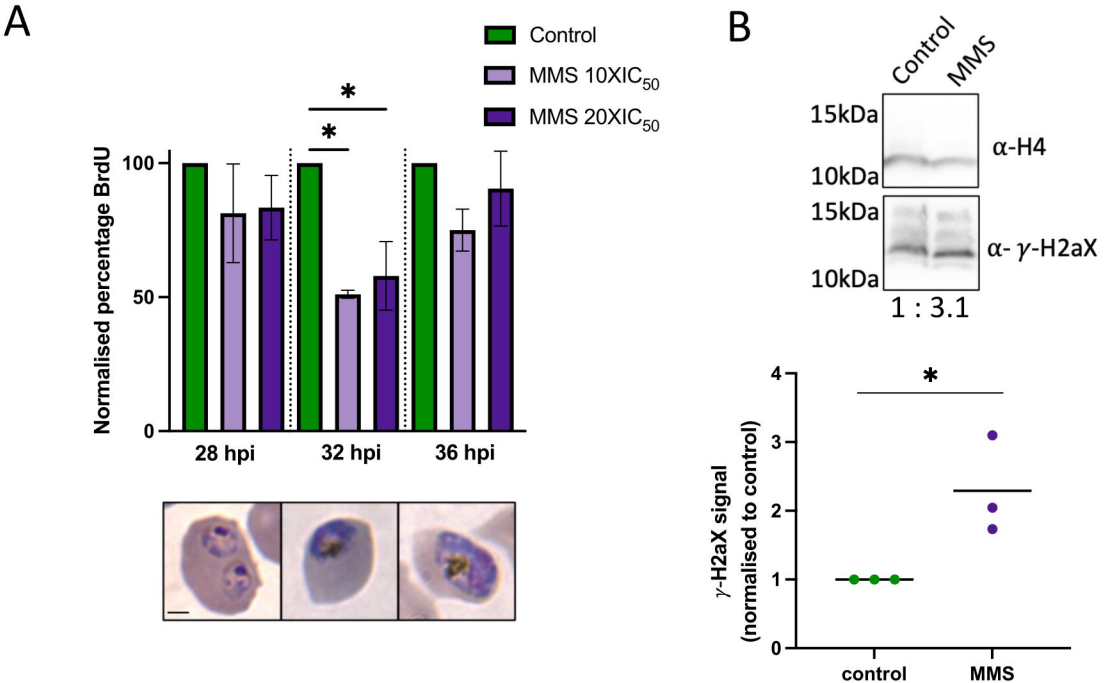
A
Control
MMS 10XIC50
MMS 20XIC50
*
*
Normalised percentage BrdU
100
50
0
28 hpi
32 hpi
36 hpi
B
Control
MMS
15kDa
10kDa
α-H4
15kDa
10kDa
α- γ-H2aX
1 : 3.1
*
γ-H2aX signal
(normalised to control)
4
3
2
1
0
control
MMS

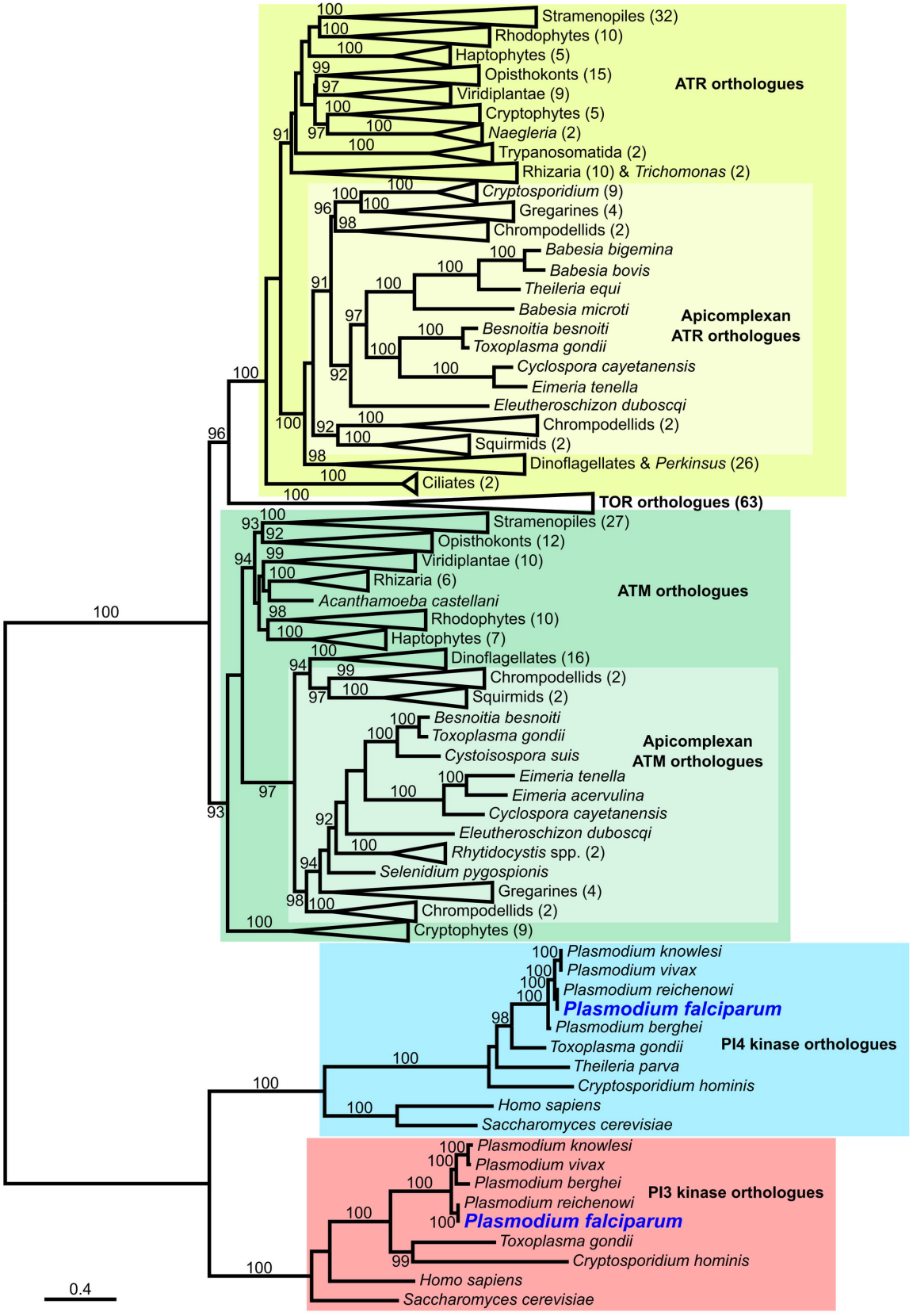
ATR orthologues
Stramenopiles (32)
Rhodophytes (10)
Haptophytes (5)
Opisthokonts (15)
Viridiplantae (9)
Cryptophytes (5)
Naegleria (2)
Trypanosomatida (2)
Rhizaria (10) & Trichomonas (2)
Cryptosporidium (9)
Gregarines (4)
Chrompodellids (2)
Apicomplexan ATR orthologues
Babesia bigemina
Babesia bovis
Theileria equi
Babesia microti
Besnoitia besnoiti
Toxoplasma gondii
Cyclospora cayetanensis
Eimeria tenella
Eleutheroschizon duboscqi
Chrompodellids (2)
Squirmids (2)
Dinoflagellates & Perkinsus (26)
Ciliates (2)
TOR orthologues (63)
ATM orthologues
Stramenopiles (27)
Opisthokonts (12)
Viridiplantae (10)
Rhizaria (6)
Acanthamoeba castellani
Rhodophytes (10)
Haptophytes (7)
Dinoflagellates (16)
Chrompodellids (2)
Squirmids (2)
Apicomplexan ATM orthologues
Besnoitia besnoiti
Toxoplasma gondii
Cystoisospora suis
Eimeria tenella
Eimeria acervulina
Cyclospora cayetanensis
Eleutheroschizon duboscqi
Rhytidocystis spp. (2)
Selenidium pygospionis
Gregarines (4)
Chrompodellids (2)
Cryptophytes (9)
PI4 kinase orthologues
Plasmodium knowlesi
Plasmodium vivax
Plasmodium reichenowi
Plasmodium falciparum
Plasmodium berghei
Toxoplasma gondii
Theileria parva
Cryptosporidium hominis
Homo sapiens
Saccharomyces cerevisiae
PI3 kinase orthologues
Plasmodium knowlesi
Plasmodium vivax
Plasmodium berghei
Plasmodium reichenowi
Plasmodium falciparum
Toxoplasma gondii
Cryptosporidium hominis
Homo sapiens
Saccharomyces cerevisiae
0.4

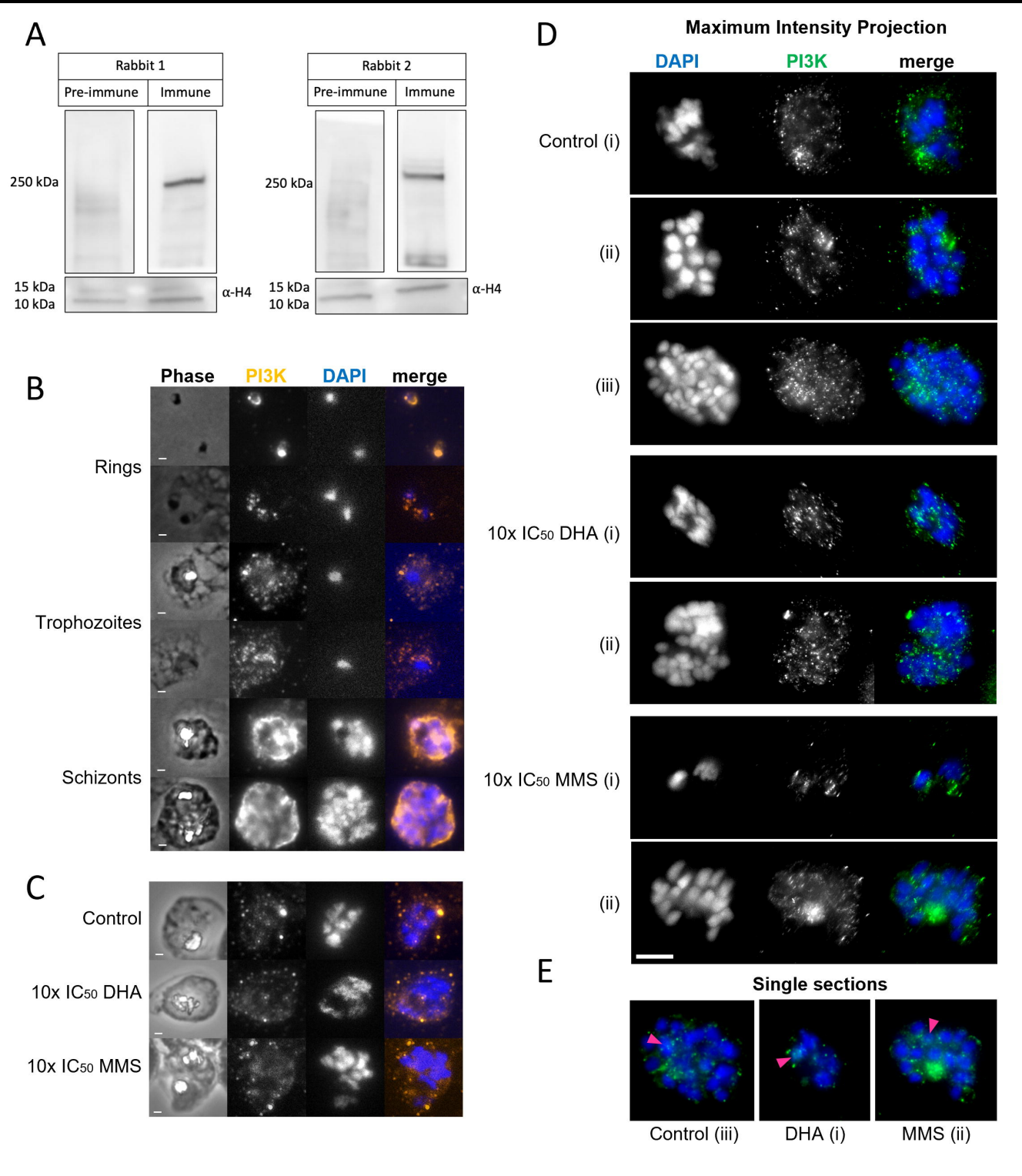
A
Rabbit 1
Pre-immune
Immune
250 kDa
15 kDa
10 kDa
α-H4
Rabbit 2
Pre-immune
Immune
250 kDa
15 kDa
10 kDa
α-H4
B
Phase
PI3K
DAPI
merge
Rings
Trophozoites
Schizonts
C
Control
10x IC50 DHA
10x IC50 MMS
D
Maximum Intensity Projection
DAPI
PI3K
merge
Control (i)
(ii)
(iii)
10x IC50 DHA (i)
(ii)
10x IC50 MMS (i)
(ii)
E
Single sections
Control (iii)
DHA (i)
MMS (ii)

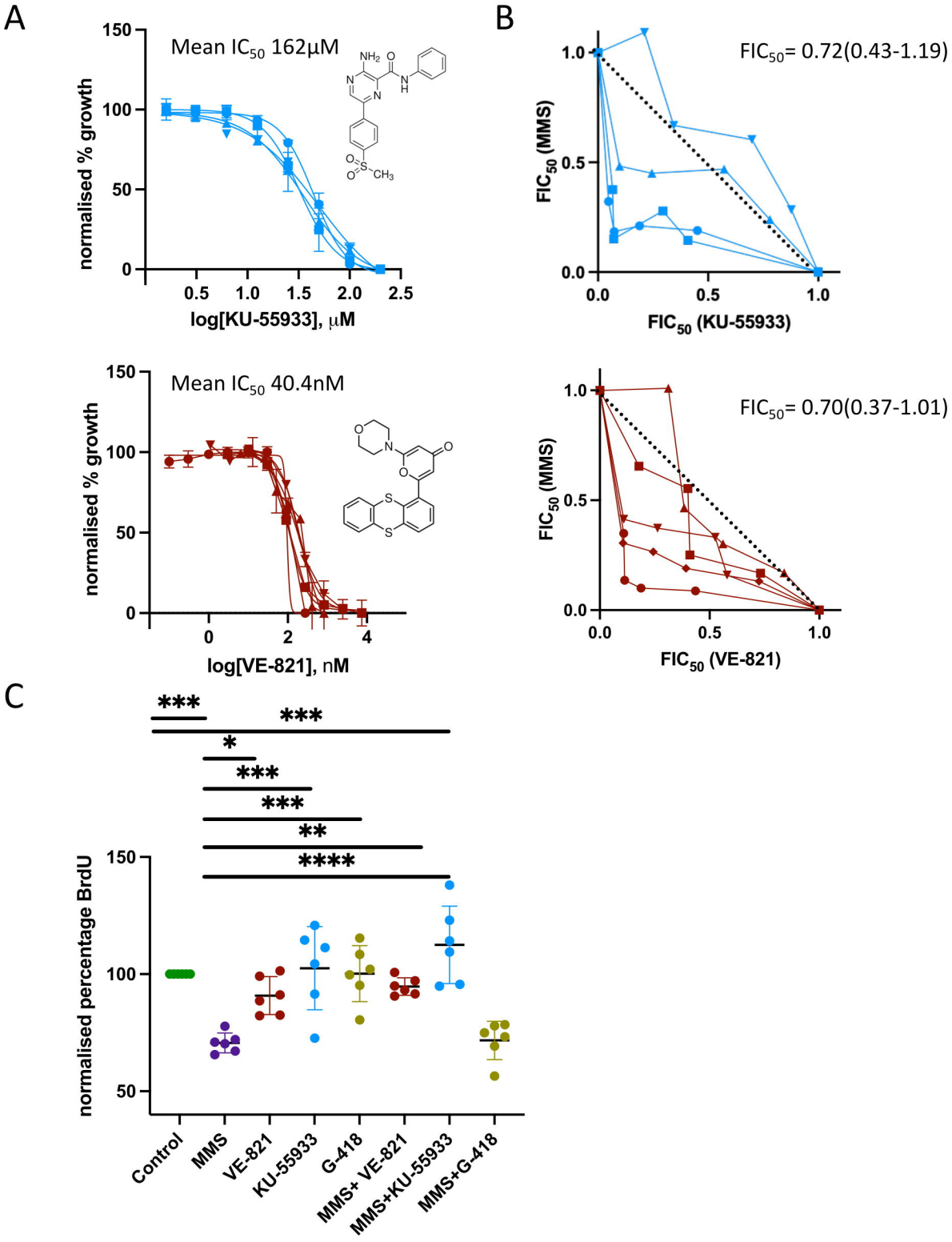
A
Mean IC50 162µM
normalised % growth
log[KU-55933], µM
B
FIC50= 0.72(0.43-1.19)
FIC50 (MMS)
FIC50 (KU-55933)
Mean IC50 40.4nM
normalised % growth
log[VE-821], nM
FIC50= 0.70(0.37-1.01)
FIC50 (MMS)
FIC50 (VE-821)
C
normalised percentage BrdU
Control
MMS
VE-821
KU-55933
G-418
MMS+ VE-821
MMS+KU-55933
MMS+G-418

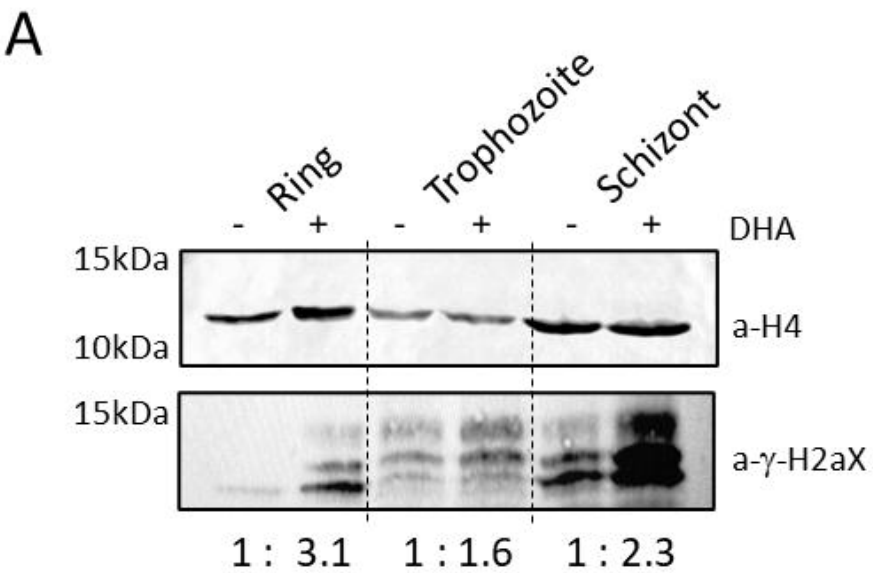
A
Ring
Trophozoite
Schizont
- + - + - +
DHA
15kDa
10kDa
a-H4
15kDa
a-γ-H2aX
1 : 3.1
1 : 1.6
1 : 2.3

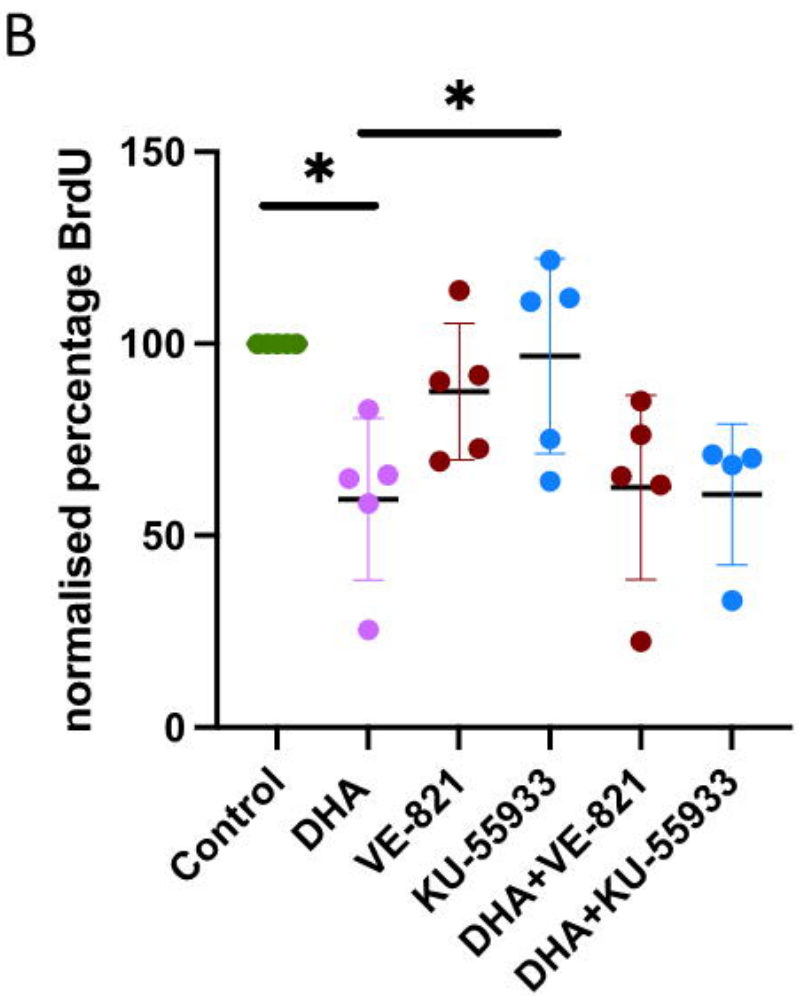
B
normalised percentage BrdU
150
100
50
0
*
*
Control
DHA
VE-821
KU-55933
DHA+VE-821
DHA+KU-55933

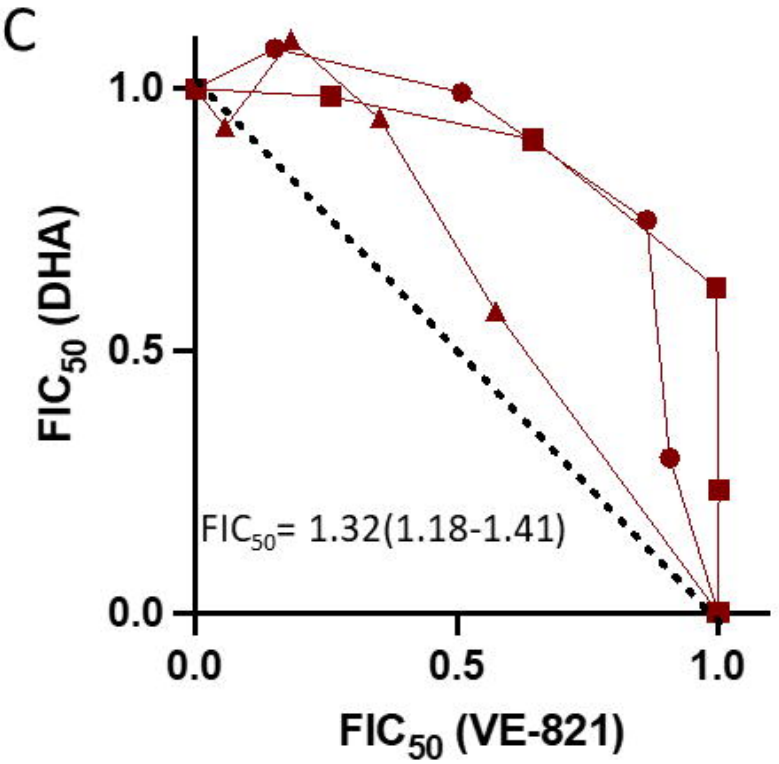
C
FIC50 (DHA)
1.0
0.5
0.0
FIC50= 1.32(1.18-1.41)
0.0
0.5
1.0
FIC50 (VE-821)

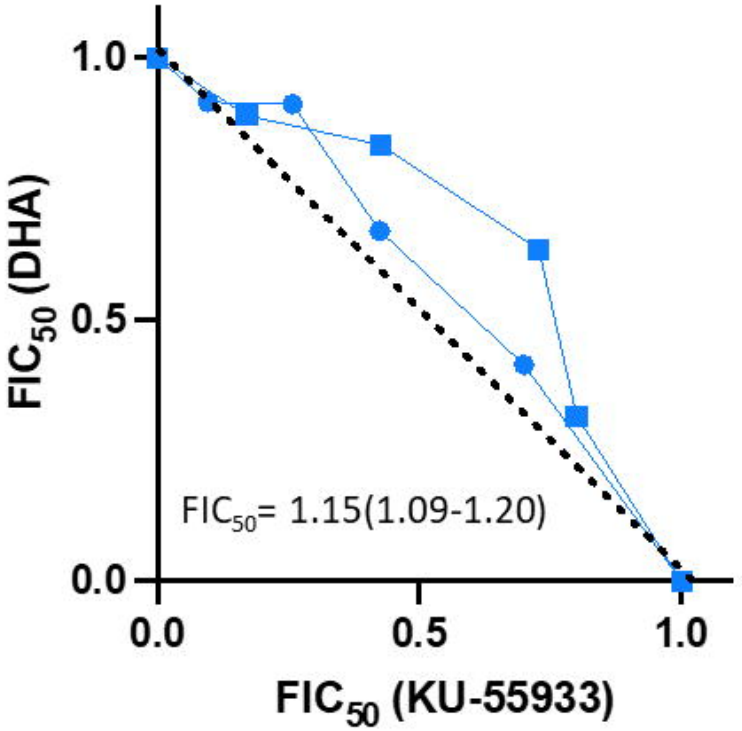
FIC50 (DHA)
1.0
0.5
0.0
FIC50= 1.15(1.09-1.20)
0.0
0.5
1.0
FIC50 (KU-55933)

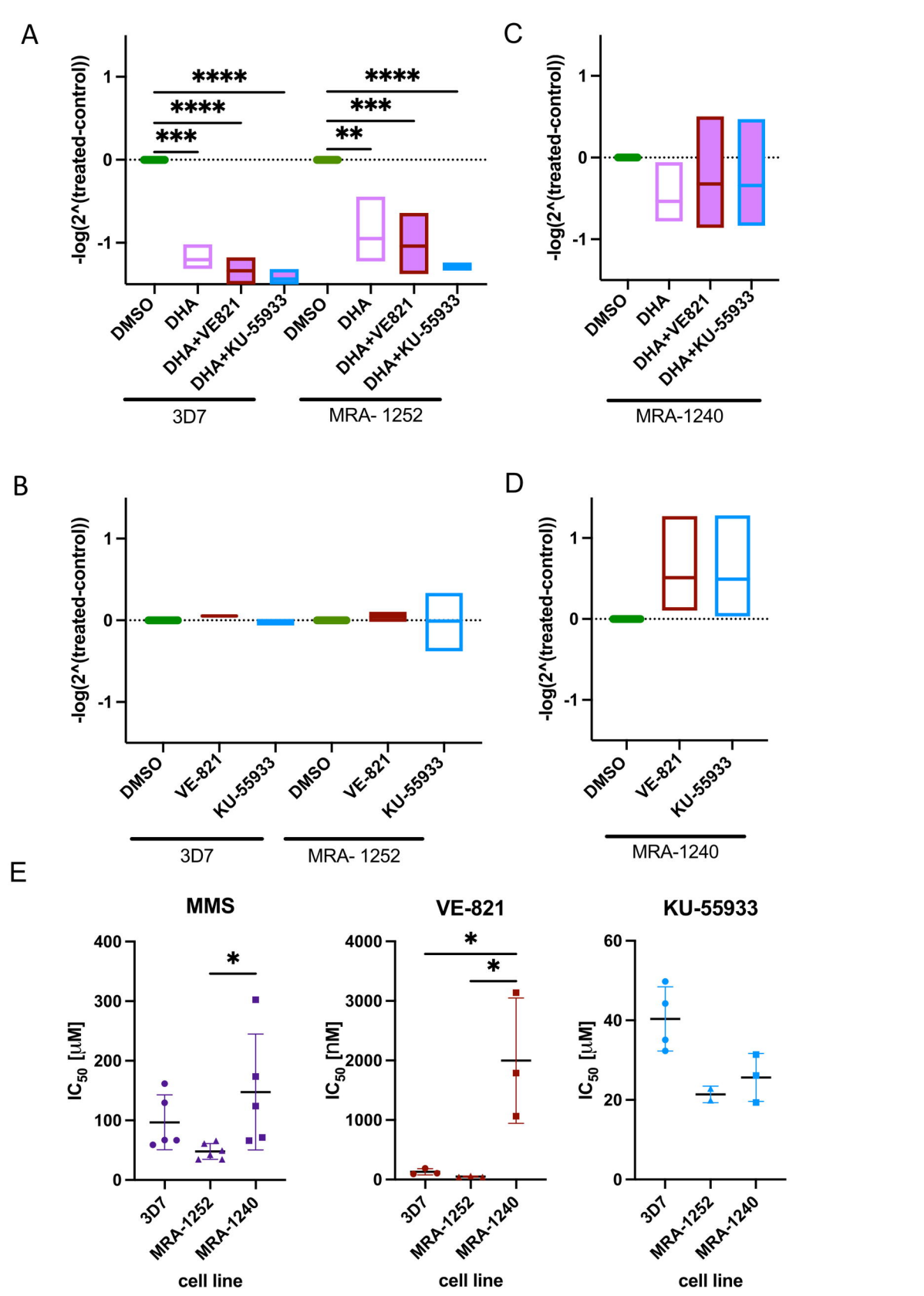
A
-log(2^(treated-control))
1
0
-1
****
****
***
****
***
**
DMSO
DHA
DHA+VE821
DHA+KU-55933
DMSO
DHA
DHA+VE821
DHA+KU-55933
3D7
MRA- 1252
C
-log(2^(treated-control))
1
0
-1
DMSO
DHA
DHA+VE821
DHA+KU-55933
MRA-1240
B
-log(2^(treated-control))
1
0
-1
DMSO
VE-821
KU-55933
DMSO
VE-821
KU-55933
3D7
MRA- 1252
D
-log(2^(treated-control))
1
0
-1
DMSO
VE-821
KU-55933
MRA-1240
E
MMS
IC50 [µM]
400
300
200
100
0
*
3D7
MRA-1252
MRA-1240
cell line
VE-821
IC50 [nM]
4000
3000
2000
1000
0
*
*
3D7
MRA-1252
MRA-1240
cell line
KU-55933
IC50 [µM]
60
40
20
0
3D7
MRA-1252
MRA-1240
cell line